

Mechanical annealing of model glasses: Effects of strain amplitude and temperature

Nikolai V. Priezjev^{1,2}

¹*Department of Mechanical and Materials Engineering,*

Wright State University, Dayton, OH 45435 and

²*National Research University Higher School of Economics, Moscow 101000, Russia*

(Dated: December 2, 2021)

Abstract

Molecular dynamics simulations are performed to examine the dynamic response of amorphous solids to oscillatory shear at finite temperatures. The data were collected from a poorly annealed binary glass, which was deformed periodically in the elastic regime during several hundred shear cycles. We found that the characteristic time required to reach a steady state with a minimum potential energy is longer at higher temperatures and larger strain amplitudes. With decreasing strain amplitude, the asymptotic value of the potential energy increases but it remains lower than in quiescent samples. The transient decay of the potential energy correlates well with a gradual decrease in the volume occupied by atoms with large nonaffine displacements. By contrast, the maximum amplitude of shear stress oscillations is attained relatively quickly when a large part of the system starts to deform reversibly.

PACS numbers: 62.20.F-, 61.43.Fs, 83.10.Rs

I. INTRODUCTION

The mechanical properties of metallic glasses can be tailored by designing and exploring various thermomechanical processing routes [1]. It is generally accepted that in contrast to crystalline materials where deformation under applied forces can be understood via motion of topological line defects, the plastic deformation in glassy systems involves highly localized rearrangements of small groups of atoms [2, 3]. Atomistic simulation studies have shown that metallic glasses typically fail by forming shear bands under either monotonic [4, 5] or cyclic loading [6–8] conditions. It was recently demonstrated that during cyclic indentation loading even within the nominal elastic regime, metallic glasses can be hardened due to atomic-level structural changes that lead to stiffening in regions of the otherwise preferred yielding path [9–11]. However, the effects of hardening and softening in metallic glasses during time-dependent deformation protocol remain relatively unexplored.

In recent years, the dynamic response of disordered systems to periodic shear strain deformation was extensively studied via molecular dynamics simulations [7, 12–23] and experimental measurements [24–29]. Notably, it was shown that during oscillatory athermal quasistatic deformation below yield, amorphous solids evolve into periodic limit cycles with reversible particle dynamics, while above the critical strain amplitude, the system dynamics becomes chaotic with a positive maximal Lyapunov exponent [14, 16]. Interestingly, the characteristic time needed to reach a steady state in periodically sheared particle suspensions diverges at the critical strain amplitude [26]. Furthermore, the analysis of the avalanche statistics and percolation characteristics in a model glass under periodic quasistatic loading suggests that yielding is a first-order phase transition, and the asymptotic potential energy per particle at strain amplitudes below the elastic limit depends on the sample preparation history [13, 20]. At finite temperatures, a slowly annealed glass subjected to a small-amplitude periodic shear remains in a state with a low potential energy; while near the critical strain amplitude, after a number of shear cycles, the formation of a shear band is detected, which is associated with a sharp increase in the potential energy and with a distinct drop in the amplitude of shear stress oscillations [7, 18]. Nevertheless, the effects of cooling rate, strain amplitude, period of oscillations and temperature on the atomic structure and potential energy in glassy systems remain not fully understood.

In this paper, the dynamic behavior of a model glass subjected to slow oscillatory shear

is investigated using molecular dynamics simulations. It will be shown that poorly annealed binary glasses, periodically deformed below yield, attain states with a potential energy that is lower (higher) than that in quiescent glasses prepared with a fast (slow) cooling rate. Upon increasing strain amplitude or temperature, the characteristic time to reach a steady state increases from a few tens to hundreds of shear cycles. It is also found that particles with large nonaffine displacements initially form large clusters whose sizes gradually decay with increasing number of cycles until the potential energy levels off to a constant value.

The rest of the paper is structured as follows. The description of molecular dynamics simulations is provided in the next section. The time series of the potential energy and shear stress at different temperatures and strain amplitudes as well as the analysis of nonaffine displacements are presented in Sec. III. A brief summary of the results is given in the last section.

II. MOLECULAR DYNAMICS SIMULATION MODEL

The model system we study is a three-dimensional (80:20) binary mixture originally developed by Kob and Andersen [30] in order to reproduce the properties of the metal alloy Ni₈₀P₂₀ [31]. In this model, the interaction between two nearby atoms is described by the truncated Lennard-Jones (LJ) potential:

$$V_{\alpha\beta}(r) = 4\varepsilon_{\alpha\beta} \left[\left(\frac{\sigma_{\alpha\beta}}{r} \right)^{12} - \left(\frac{\sigma_{\alpha\beta}}{r} \right)^6 \right], \quad (1)$$

where the interaction parameters are set to $\varepsilon_{AA} = 1.0$, $\varepsilon_{AB} = 1.5$, $\varepsilon_{BB} = 0.5$, $\sigma_{AB} = 0.8$, $\sigma_{BB} = 0.88$, and $m_A = m_B$ [30]. This parametrization ensures that the system will not be crystallized at low temperatures [30]. For computational efficiency, the cutoff radius is fixed $r_{c,\alpha\beta} = 2.5\sigma_{\alpha\beta}$. In what follows, the LJ units of length, mass, energy, and time are set to $\sigma = \sigma_{AA}$, $m = m_A$, $\varepsilon = \varepsilon_{AA}$, and $\tau = \sigma\sqrt{m/\varepsilon}$, respectively. The Newton's equations of motion were integrated numerically using the velocity Verlet algorithm [32, 33] with the time step $\Delta t_{MD} = 0.005\tau$.

The system consists of $N = 60\,000$ atoms that were placed in a periodic box of linear size $L = 36.84\sigma$ (see Fig. 1). The MD simulations were performed at a constant volume with the corresponding density $\rho = \rho_A + \rho_B = 1.2\sigma^{-3}$. Initially, the system was equilibrated in the absence of deformation at a high temperature of $1.1\varepsilon/k_B$, which is above the crit-

ical temperature $T_c \approx 0.435 \varepsilon/k_B$ [30]. Throughout the study, k_B denotes the Boltzmann constant. In our setup, the temperature was regulated by the dissipative particle dynamics (DPD) thermostat, which is known to stabilize the numerical integration of the equations of motion and to avoid profile biasing in nonequilibrium simulations [34].

In order to avoid the formation of a shear band at the initial stage of the deformation protocol (described below), the system was instantaneously quenched from a high temperature phase at $T_{LJ} = 1.1 \varepsilon/k_B$ to a low temperature $T_{LJ} = 10^{-2} \varepsilon/k_B$ and kept undeformed at this temperature during the time interval of 100τ . Then, the time-periodic shear strain deformation was applied along the xz plane by using the Lees-Edwards periodic boundary conditions and the SLLOD algorithm [35] as follows:

$$\gamma(t) = \gamma_0 \sin(2\pi t/T), \quad (2)$$

where γ_0 is the strain amplitude and T is the oscillation period. In this study, all simulations were performed with the oscillation period $T = 5000 \tau$ and the oscillation frequency $\omega = 2\pi/T = 1.26 \times 10^{-3} \tau^{-1}$. During production runs, atom positions were saved at the end of each cycle, while the potential energy and shear stress were computed every 5τ . Due to the relatively large system size and implementation of the DPD thermostat, where stochastic forces have to be generated for all pairs of nearby particles, the MD simulations become computationally demanding. For example, a typical simulation of 40 oscillation cycles using 32 parallel processors required about 110 hours. Thus, the data were collected only in one sample at temperatures $T_{LJ} k_B/\varepsilon = 10^{-2}, 10^{-3}, 10^{-4}, 10^{-5}$ and 10^{-6} .

III. RESULTS

It has long been realized that mechanical properties of glassy materials depend crucially on the sample preparation history [36]. In general, a slower thermal annealing process allows for a thorough exploration of the potential energy landscape, so that the system can find a deeper energy minimum, and, as a result, upon external deformation, the dynamical yield stress becomes larger [37]. It was further shown that the yield stress depends logarithmically on both the aging time and the imposed shear rate [38]. In this study, we prepare poorly annealed binary glass and periodically deform it below the yield point at low temperatures. Under cyclic loading, the potential energy landscape can be significantly distorted, which in

turn might promote plastic rearrangements, and upon reversal the system can be relocated to deeper energy minima [39]. Although it is intuitively expected that thermal fluctuations might facilitate irreversible rearrangements of groups of atoms in a deformed glass; however, the combined effect of temperature and strain amplitude on the annealing process remains difficult to predict.

The time series of the potential energy per particle are presented in Fig. 2 during 600 shear cycles for the selected strain amplitudes and temperature $T_{LJ} = 10^{-2} \varepsilon/k_B$. It can be observed that at each strain amplitude the minimum of the potential energy gradually decreases with increasing number of cycles and then levels off to constant values for $\gamma_0 \leq 0.05$. Moreover, the time interval needed to reach steady state becomes larger with increasing strain amplitude. However, at finite temperatures it is difficult to determine the exact number of shear cycles in the transient regime. For example, one can notice in Fig. 2 that at the strain amplitude $\gamma_0 = 0.04$, the potential energy nearly saturates to a constant value after about 200 cycles, which is followed by a small drop in the potential energy at about 300 cycles. It is also evident from Fig. 2 that at large strain amplitudes, $\gamma_0 = 0.06$ and 0.07 , the transient regime exceeds 600 cycles.

As illustrated in Fig. 3, similar trends in the decay of the potential energy can be observed at the lower temperature $T_{LJ} = 10^{-5} \varepsilon/k_B$. It can be seen that at a given strain amplitude, the transient regime of oscillations is shorter than in the case $T_{LJ} = 10^{-2} \varepsilon/k_B$ reported in Fig. 2. Based on the results for $T_{LJ} \leq 10^{-2} \varepsilon/k_B$, we thus conclude that transition to the steady state regime of elastic deformation occurs faster at lower temperatures. We further comment that the minimum value of the potential energy is lower for the strain amplitude $\gamma_0 = 0.07$ at $T_{LJ} = 10^{-5} \varepsilon/k_B$ than for $\gamma_0 = 0.07$ at $T_{LJ} = 10^{-2} \varepsilon/k_B$ (note that the vertical scales are the same in Figs. 2 and 3). Interestingly, the data shown for $\gamma_0 = 0.07$ in Fig. 3 indicate that the potential energy after about 400 cycles approaches a constant value with superimposed fluctuations, which suggests the presence of irreversible plastic events during periodic deformation. By contrast, the minima of the potential energy at each cycle are nearly the same in the steady regime at strain amplitudes $\gamma_0 \leq 0.06$, which is indicative of reversible dynamics after each shear cycle (to be discussed below). This behavior is similar to that reported in athermal, quasistatic oscillatory shear simulations of amorphous systems, which after some time were found to settle into reversible limit cycles [14, 16].

The variation of shear stress during 600 cycles at different strain amplitudes are shown for $T_{LJ} = 10^{-2} \varepsilon/k_B$ in Fig. 4 and for $T_{LJ} = 10^{-5} \varepsilon/k_B$ in Fig. 5. It is clearly seen that the amplitude of shear stress oscillations in the steady regime is larger at higher strain amplitudes. Somewhat surprisingly, we find that the number of periods required to reach the maximum amplitude of shear stress oscillations at a given γ_0 is significantly smaller than the transient time for the variation of minima of the potential energy reported in Figs. 2 and 3. This difference is largest in the cases $\gamma_0 = 0.06$ and 0.07 at $T_{LJ} = 10^{-2} \varepsilon/k_B$, where the amplitude of shear stress saturates after about 100 cycles, while the systems continue to explore states with progressively lower potential energy minima during 600 cycles.

The summary of the data for the maximum amplitude of shear stress and minimum of the potential energy at different temperatures and strain amplitudes are presented in Fig. 6. As is evident, both quantities U_{min} and σ_{xz}^{max} are nearly independent of temperature, except for the potential energy at the strain amplitude $\gamma_0 = 0.07$ and $T_{LJ} = 10^{-2} \varepsilon/k_B$. The effect of cyclic loading on U_{min} can be estimated by performing an instantaneous quench from $T_{LJ} = 1.1 \varepsilon/k_B$ to a low temperature in the range $10^{-5} \varepsilon/k_B \leq T_{LJ} \leq 10^{-2} \varepsilon/k_B$ in the absence of shear. Such a protocol yields a distinctly higher value of the potential energy, $U \approx -8.21 \varepsilon$, than those reported in Fig. 6. On the other hand, it was previously shown [7, 18] that a slow annealing of an undeformed system across the glass transition with the rate of $10^{-5} \varepsilon/k_B \tau$ to the target temperature $T_{LJ} = 10^{-2} \varepsilon/k_B$ results in the potential energy $U \approx -8.31 \varepsilon$, which is markedly lower than U_{min} for all γ_0 in Fig. 6. These results are consistent with the conclusions obtained for the binary glass model using athermal quasistatic oscillatory shear deformation in the elastic range [20].

Additional insight into the relaxation process under periodic deformation can be gained through the analysis of the so-called nonaffine displacements of atoms. To remind, the relative displacements of atoms within a small group can be described by a combination of a linear transformation and a deviation from a local linear field [3]. Thus, the nonaffine measure can be computed using the transformation matrix \mathbf{J}_i that best maps all vectors between the i -th atom and its neighbors during the time interval Δt according to:

$$D^2(t, \Delta t) = \frac{1}{N_i} \sum_{j=1}^{N_i} \left\{ \mathbf{r}_j(t + \Delta t) - \mathbf{r}_i(t + \Delta t) - \mathbf{J}_i [\mathbf{r}_j(t) - \mathbf{r}_i(t)] \right\}^2, \quad (3)$$

where the summation is performed over N_i neighboring atoms within the cutoff distance of

1.5σ from $\mathbf{r}_i(t)$. Note that, when normalized by the number of neighbors, the value $D^2 \approx 0.01\sigma^2$ is equal to the typical cage size, and, therefore, nonaffine displacements with $D^2 \gtrsim 0.01\sigma^2$ correspond to cage breaking events, which in some cases can be reversible [17, 18]. In particular, the analysis of spatial configurations of atoms with large nonaffine displacements allowed a clear identification of a system-spanning shear band, which was spontaneously formed after a number of shear cycles at the critical strain amplitude in a well-annealed binary glass [7].

In our analysis, the nonaffine measure was evaluated numerically based on atom positions at the beginning and the end of each cycle at zero global strain. Typically, the quantity D^2 is broadly distributed even at small strain amplitudes with the majority of atoms undergoing reversible displacements with $D^2 < 0.01\sigma^2$ due to thermal fluctuations [7, 17, 18]. Therefore, in what follows, we only plot positions of atoms with $D^2(nT, T) > 0.01\sigma^2$, where n is the cycle number. Four sets of time sequences of spatial configurations of atoms with large nonaffine displacements during a complete cycle are displayed in Figs. 7 and 8 for $\gamma_0 = 0.06$ and 0.07 at $T_{LJ} = 10^{-2} \varepsilon/k_B$ and in Figs. 9 and 10 for $\gamma_0 = 0.06$ and 0.07 at $T_{LJ} = 10^{-5} \varepsilon/k_B$. In each case, the atoms with $D^2 > 0.01\sigma^2$ form clusters whose sizes gradually decay with increasing number of cycles. Notice that after 80 cycles, the atoms with small nonaffine displacements (empty volume in Figs. 7-10) are organized into percolating regions that can deform elastically and support relatively large shear stress. This might explain why the shear stress amplitude rather quickly approaches a constant value, as shown in Figs. 4 and 5. At the same time, progressively lower minima of the potential energy can still be attained via small-scale plastic rearrangements leading to extended transients shown in Figs. 2 and 3. We finally comment that at lower strain amplitudes, $\gamma_0 \leq 0.05$, the sequence of atom configurations with large nonaffine displacements appears to be qualitatively very similar to the one shown in Fig. 9, where large clusters rapidly disappear during the first few tens of cycles followed by, in some cases, a few isolated rearrangements in the steady regime of periodic deformation.

IV. CONCLUSIONS

In summary, large-scale molecular dynamics simulations were carried out to investigate the influence of strain amplitude and temperature on relaxation dynamics of a model glass.

We considered a three-dimensional binary mixture with highly nonadditive interaction parameters that prevent crystallization at low temperatures and used the dissipative particle dynamics thermostat that does not couple particle dynamics to flow profile. The system was initially prepared at a high temperature well above the glass transition, and then following a fast quench to low temperature at constant volume, the glass was subjected to periodic shear during hundreds of cycles.

It was found that at strain amplitudes below yield, the system gradually evolves in a steady state with the potential energy that is higher (lower) than that in a very slowly (quickly) annealed glass in the absence of deformation. Moreover, with increasing strain amplitude, the system is ultimately relocated to deeper energy minima, and the characteristic time required to reach steady state becomes longer at larger strain amplitudes and/or higher temperatures. Furthermore, the analysis of nonaffine displacements indicates that after the first few tens of shear cycles, a large part of the system starts to deform reversibly, which correlates with the maximum amplitude of shear stress oscillations. On the other hand, small-scale plastic rearrangements are associated with extended transients before reaching steady state with a minimum potential energy.

Acknowledgments

Financial support from the National Science Foundation (CNS-1531923) is gratefully acknowledged. The study has been in part funded by the Russian Academic Excellence Project ‘5-100’. The molecular dynamics simulations were performed using the efficient parallel code LAMMPS developed at Sandia National Laboratories [32]. This work was supported in part by Michigan State University through computational resources provided by the Institute for Cyber-Enabled Research.

-
- [1] T. Egami, T. Iwashita, and W. Dmowski, Mechanical properties of metallic glasses, *Metals* **3**, 77 (2013).
 - [2] A. S. Argon, Plastic deformation in metallic glasses, *Acta Metall.* **27**, 47 (1979).
 - [3] M. L. Falk and J. S. Langer, Dynamics of viscoplastic deformation in amorphous solids, *Phys.*

- Rev. E **57**, 7192 (1998).
- [4] Y. Shi and M. L. Falk, Atomic-scale simulations of strain localization in three-dimensional model amorphous solids, *Phys. Rev. B* **73**, 214201 (2006).
 - [5] G. P. Shrivastav, P. Chaudhuri, and J. Horbach, Yielding of glass under shear: A directed percolation transition precedes shear-band formation, *Phys. Rev. E* **94**, 042605 (2016).
 - [6] Z. D. Sha, S. X. Qu, Z. S. Liu, T. J. Wang, and H. Gao, Cyclic deformation in metallic glasses, *Nano Lett.* **15**, 7010 (2015).
 - [7] N. V. Priezjev, Collective nonaffine displacements in amorphous materials during large-amplitude oscillatory shear, *Phys. Rev. E* **95**, 023002 (2017).
 - [8] Z. Sha, W. H. Wong, Q. Pei, P. S. Branicio, Z. Liu, T. Wang, T. Guo, H. Gao, Atomistic origin of size effects in fatigue behavior of metallic glasses, *J. Mech. Phys. Solids* **104**, 84 (2017).
 - [9] C. E. Packard, L. M. Witmer, and C. A. Schuh, Hardening of a metallic glass during cyclic loading in the elastic range, *Appl. Phys. Lett.* **92**, 171911 (2008).
 - [10] C. Deng and C. A. Schuh, Atomistic mechanisms of cyclic hardening in metallic glass, *Appl. Phys. Lett.* **100**, 251909 (2012).
 - [11] D. Zhao, H. Zhao, B. Zhu, and S. Wang, Investigation on hardening behavior of metallic glass under cyclic indentation loading via molecular dynamics simulation, *Appl. Surf. Sci.* **416**, 14 (2017).
 - [12] N. V. Priezjev, Heterogeneous relaxation dynamics in amorphous materials under cyclic loading, *Phys. Rev. E* **87**, 052302 (2013).
 - [13] D. Fiocco, G. Foffi, and S. Sastry, Oscillatory athermal quasistatic deformation of a model glass, *Phys. Rev. E* **88**, 020301(R) (2013).
 - [14] I. Regev, T. Lookman, and C. Reichhardt, Onset of irreversibility and chaos in amorphous solids under periodic shear, *Phys. Rev. E* **88**, 062401 (2013).
 - [15] N. V. Priezjev, Dynamical heterogeneity in periodically deformed polymer glasses, *Phys. Rev. E* **89**, 012601 (2014).
 - [16] I. Regev, J. Weber, C. Reichhardt, K. A. Dahmen, and T. Lookman, Reversibility and criticality in amorphous solids, *Nat. Commun.* **6**, 8805 (2015).
 - [17] N. V. Priezjev, Reversible plastic events during oscillatory deformation of amorphous solids, *Phys. Rev. E* **93**, 013001 (2016).
 - [18] N. V. Priezjev, Nonaffine rearrangements of atoms in deformed and quiescent binary glasses,

- Phys. Rev. E **94**, 023004 (2016).
- [19] T. Kawasaki and L. Berthier, Macroscopic yielding in jammed solids is accompanied by a non-equilibrium first-order transition in particle trajectories, Phys. Rev. E **94**, 022615 (2016).
- [20] P. Leishangthem, A. D. S. Parmar, and S. Sastry, The yielding transition in amorphous solids under oscillatory shear deformation, Nat. Commun. **8**, 14653 (2017).
- [21] M. Fan, M. Wang, K. Zhang, Y. Liu, J. Schroers, M. D. Shattuck, and C. S. O’Hern, The effects of cooling rate on particle rearrangement statistics: Rapidly cooled glasses are more ductile and less reversible, Phys. Rev. E **95**, 022611 (2017).
- [22] I. Regev and T. Lookman, Yield in amorphous solids: The ant in the energy landscape labyrinth, arXiv:1701.04020 (2017).
- [23] P. K. Jana, M. J. Alava, and S. Zapperi, Irreversibility transition of colloidal polycrystals under cyclic deformation, Sci. Rep. **7**, 45550 (2017).
- [24] G. Petekidis, A. Moussaid, and P. N. Pusey, Rearrangements in hard-sphere glasses under oscillatory shear strain, Phys. Rev. E **66**, 051402 (2002).
- [25] F. Rouyer, S. Cohen-Addad, R. Hohler, P. Sollich, and S. M. Fielding, The large amplitude oscillatory strain response of aqueous foam: Strain localization and full stress Fourier spectrum, Eur. Phys. J. E **27**, 309 (2008).
- [26] L. Corte, P. M. Chaikin, J. P. Gollub, and D. J. Pine, Random organization in periodically driven systems, Nature Physics **4**, 420 (2008).
- [27] E. D. Knowlton, D. J. Pine, and L. Cipelletti, A microscopic view of the yielding transition in concentrated emulsions, Soft Matter **10**, 6931 (2014).
- [28] J. Kim, D. Merger, M. Wilhelm, and M. E. Helgeson, Microstructure and nonlinear signatures of yielding in a heterogeneous colloidal gel under large amplitude oscillatory shear, J. Rheol. **58**, 1359 (2014).
- [29] B. Saint-Michel, T. Gibaud, and S. Manneville, Predicting and assessing rupture in protein gels under oscillatory shear, Soft Matter **13**, 2643 (2017).
- [30] W. Kob and H. C. Andersen, Testing mode-coupling theory for a supercooled binary Lennard-Jones mixture: The van Hove correlation function, Phys. Rev. E **51**, 4626 (1995).
- [31] T. A. Weber and F. H. Stillinger, Local order and structural transitions in amorphous metal-metalloid alloys, Phys. Rev. B **31**, 1954 (1985).
- [32] S. J. Plimpton, Fast parallel algorithms for short-range molecular dynamics, J. Comp. Phys.

- 117, 1 (1995).
- [33] M. P. Allen and D. J. Tildesley, *Computer Simulation of Liquids* (Clarendon, Oxford, 1987).
 - [34] T. Soddemann, B. Dunweg, and K. Kremer, Dissipative particle dynamics: A useful thermostat for equilibrium and nonequilibrium molecular dynamics simulations, *Phys. Rev. E* **68**, 046702 (2003).
 - [35] D. J. Evans and G. P. Morriss, *Statistical Mechanics of Nonequilibrium Liquids* (Academic Press, London, 1990).
 - [36] G. Kumar, P. Neibecker, Y. H. Liu, and J. Schroers, Critical fictive temperature for plasticity in metallic glasses, *Nat. Commun.* **4**, 1536 (2013).
 - [37] Ashwin J., E. Bouchbinder, and I. Procaccia, Cooling-rate dependence of the shear modulus of amorphous solids, *Phys. Rev. E* **87**, 042310 (2013).
 - [38] F. Varnik, L. Bocquet, and J.-L. Barrat, A study of the static yield stress in a binary Lennard-Jones glass, *J. Chem. Phys.* **120**, 2788 (2004).
 - [39] D. J. Lacks and M. J. Osborne, Energy landscape picture of overaging and rejuvenation in a sheared glass, *Phys. Rev. Lett.* **93**, 255501 (2004).

Figures

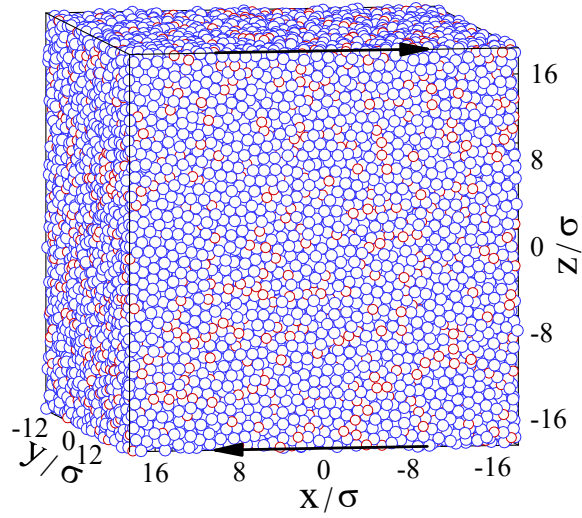


FIG. 1: (Color online) An instantaneous atom configuration of the binary Lennard-Jones glass at the temperature $T_{LJ} = 10^{-2} \varepsilon/k_B$ after 600 shear cycles with the strain amplitude $\gamma_0 = 0.06$ and oscillation period $T = 5000 \tau$. The black arrows indicate the plane of shear. Two types of atoms of different sizes are denoted by red and blue circles. Atoms are not drawn to scale.

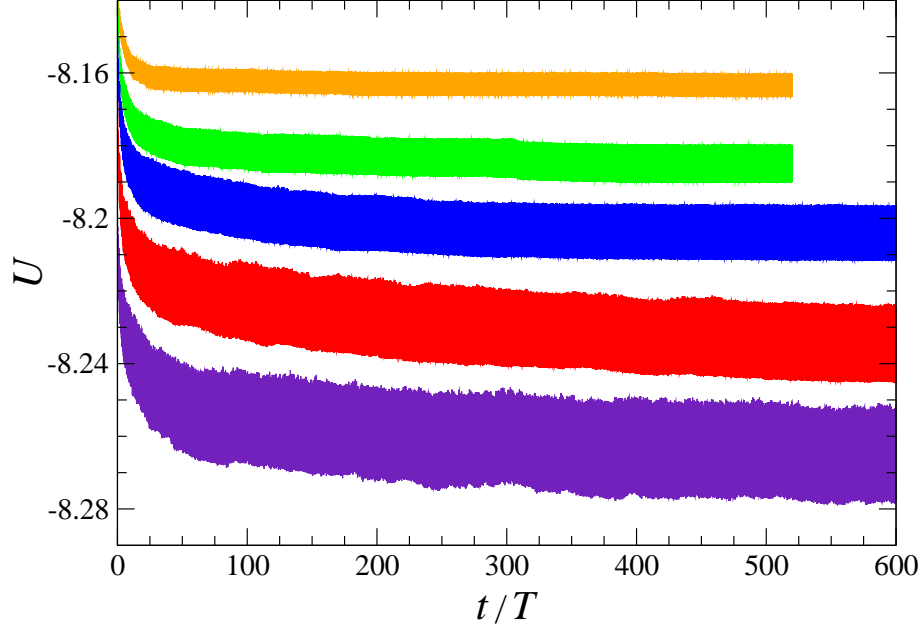


FIG. 2: (Color online) The variation of the potential energy per particle U (in units of ε) at $T_{LJ} = 10^{-2} \varepsilon/k_B$ during 600 oscillation cycles for the strain amplitudes $\gamma_0 = 0.03, 0.04, 0.05, 0.06,$ and 0.07 (from top to bottom). For clarity, the data were displaced vertically by 0.07ε for $\gamma_0 = 0.03$, by 0.06ε for $\gamma_0 = 0.04$, by 0.05ε for $\gamma_0 = 0.05$, and by 0.03ε for $\gamma_0 = 0.06$. The oscillation period is $T = 5000 \tau$.

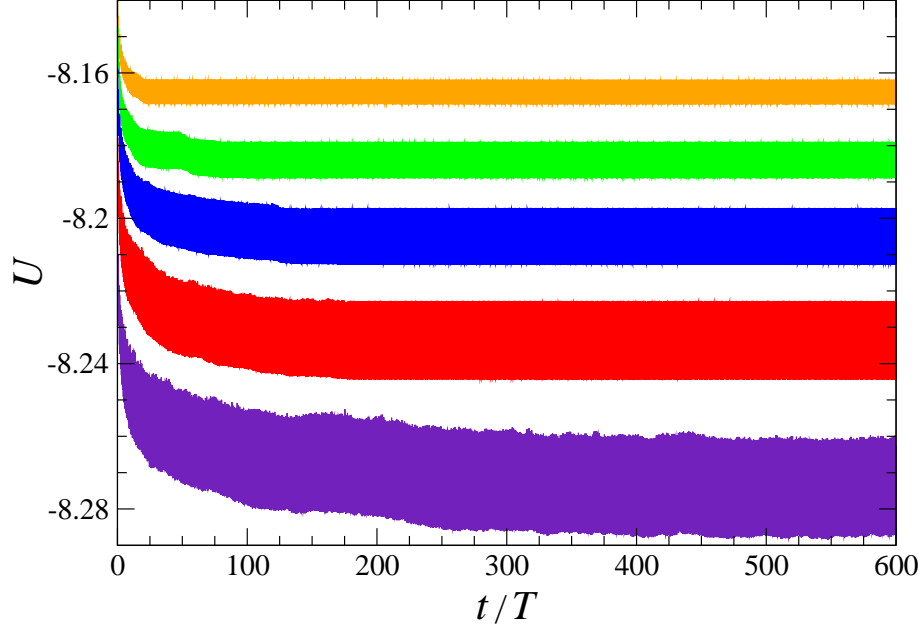


FIG. 3: (Color online) The time dependence of the potential energy per particle U (in units of ε) at the temperature $T_{LJ} = 10^{-5} \varepsilon/k_B$ during 600 oscillation cycles with the period $T = 5000 \tau$ for $\gamma_0 = 0.03, 0.04, 0.05, 0.06$, and 0.07 (from top to bottom). As in Fig. 2, the data were shifted upward by 0.07ε for $\gamma_0 = 0.03$, by 0.06ε for $\gamma_0 = 0.04$, by 0.05ε for $\gamma_0 = 0.05$, and by 0.03ε for $\gamma_0 = 0.06$.

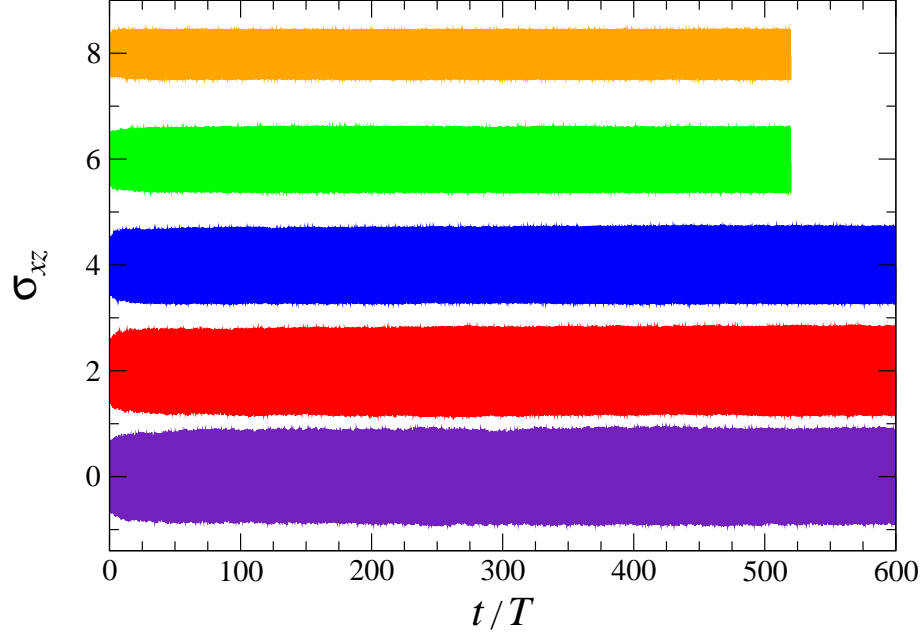


FIG. 4: (Color online) The shear stress σ_{xz} (in units of $\varepsilon\sigma^{-3}$) at the temperature $T_{LJ} = 10^{-2} \varepsilon/k_B$ for the strain amplitudes $\gamma_0 = 0.03, 0.04, 0.05, 0.06,$ and 0.07 (from top to bottom). For visualization, the data were displaced upward by $8.0 \varepsilon\sigma^{-3}$ for $\gamma_0 = 0.03$, by $6.0 \varepsilon\sigma^{-3}$ for $\gamma_0 = 0.04$, by $4.0 \varepsilon\sigma^{-3}$ for $\gamma_0 = 0.05$, and by $2.0 \varepsilon\sigma^{-3}$ for $\gamma_0 = 0.06$. The period of oscillation is $T = 5000 \tau$.

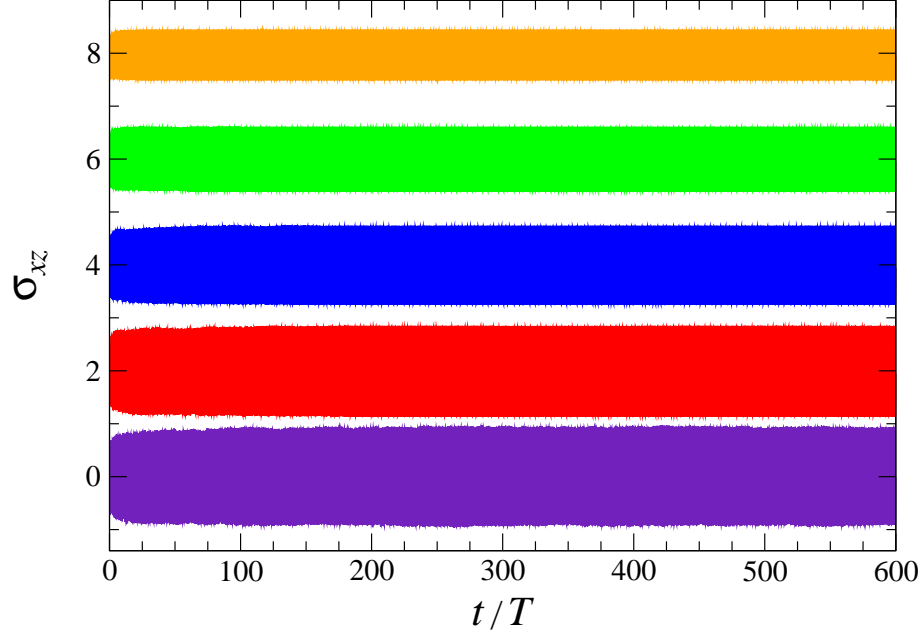


FIG. 5: (Color online) The dependence of shear stress σ_{xz} (in units of $\varepsilon\sigma^{-3}$) at $T_{LJ} = 10^{-5} \varepsilon/k_B$ as a function of time for the strain amplitudes $\gamma_0 = 0.03, 0.04, 0.05, 0.06,$ and 0.07 (from top to bottom). Similar to Fig. 4, the data were displaced by $8.0 \varepsilon\sigma^{-3}$ for $\gamma_0 = 0.03$, by $6.0 \varepsilon\sigma^{-3}$ for $\gamma_0 = 0.04$, by $4.0 \varepsilon\sigma^{-3}$ for $\gamma_0 = 0.05$, and by $2.0 \varepsilon\sigma^{-3}$ for $\gamma_0 = 0.06$.

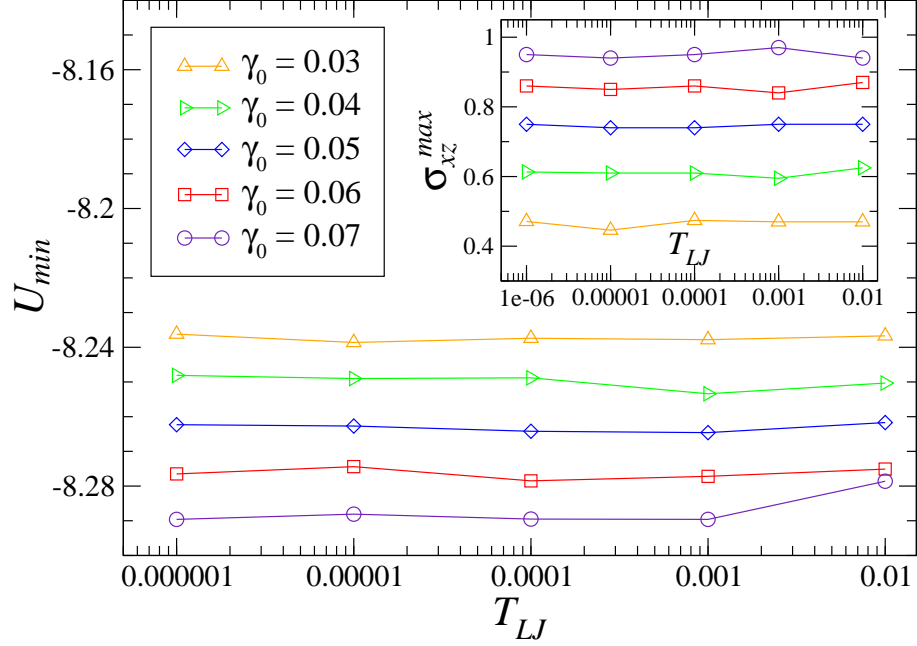


FIG. 6: (Color online) The minimum of the potential energy per particle U_{min} (in units of ε) as a function of temperature for the indicated values of the strain amplitude γ_0 . The inset shows the maximum shear stress σ_{xz}^{max} (in units of $\varepsilon\sigma^{-3}$) for the same strain amplitudes.

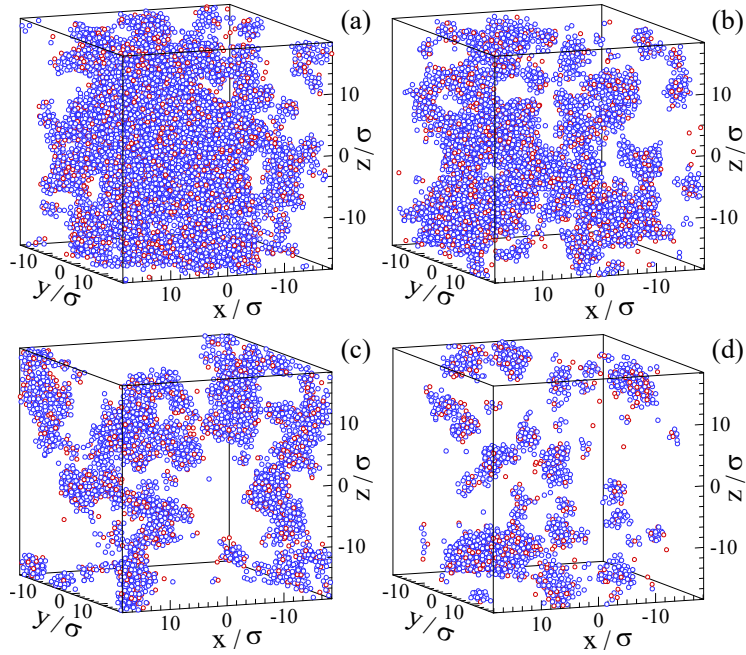


FIG. 7: (Color online) Snapshots of atom positions for the strain amplitude $\gamma_0 = 0.06$, temperature $T_{LJ} = 10^{-2} \varepsilon/k_B$, and nonaffine measure (a) $D^2(19T, T) > 0.01 \sigma^2$, (b) $D^2(79T, T) > 0.01 \sigma^2$, (c) $D^2(199T, T) > 0.01 \sigma^2$, and (d) $D^2(599T, T) > 0.01 \sigma^2$.

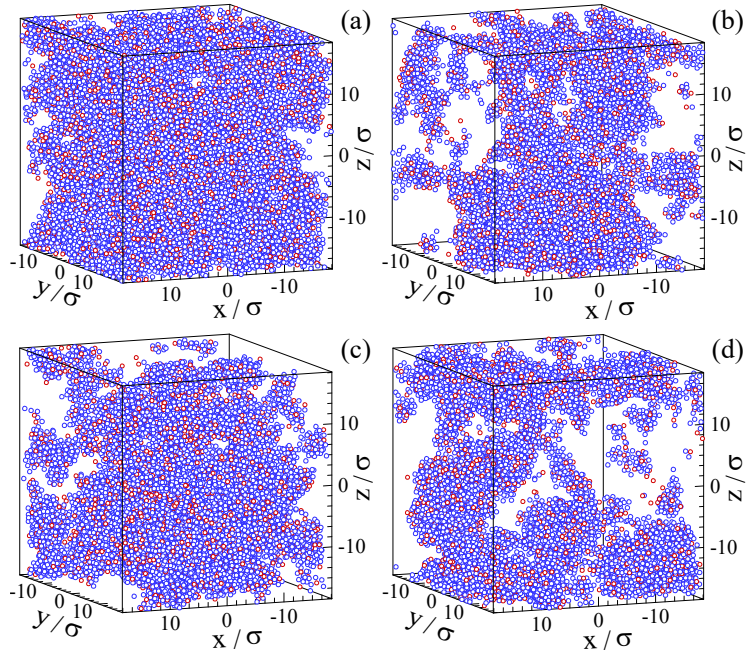


FIG. 8: (Color online) Spatial configurations of atoms for the strain amplitude $\gamma_0 = 0.07$, $T_{LJ} = 10^{-2} \varepsilon/k_B$, and nonaffine measure (a) $D^2(19T, T) > 0.01 \sigma^2$, (b) $D^2(79T, T) > 0.01 \sigma^2$, (c) $D^2(199T, T) > 0.01 \sigma^2$, and (d) $D^2(599T, T) > 0.01 \sigma^2$.

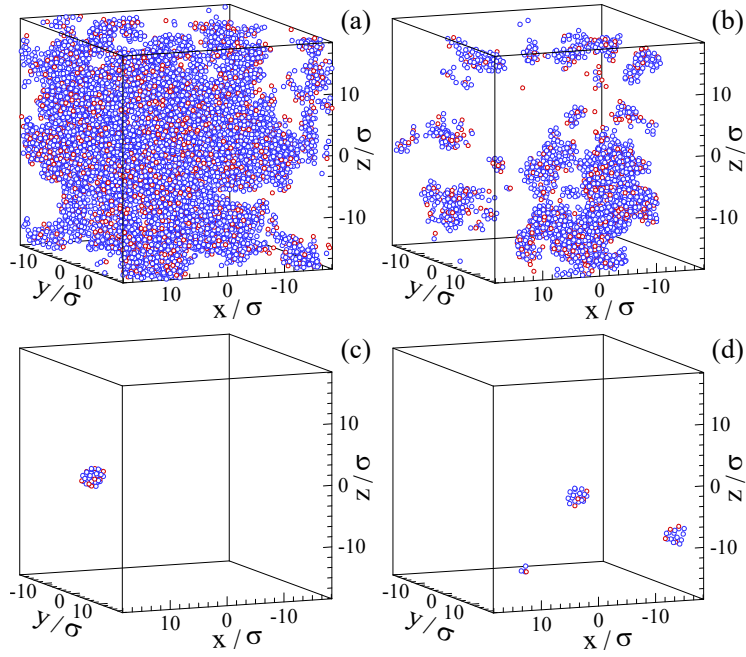


FIG. 9: (Color online) Atom positions for $\gamma_0 = 0.06$, $T_{LJ} = 10^{-5} \varepsilon/k_B$, and nonaffine measure (a) $D^2(19T, T) > 0.01 \sigma^2$, (b) $D^2(79T, T) > 0.01 \sigma^2$, (c) $D^2(199T, T) > 0.01 \sigma^2$, and (d) $D^2(599T, T) > 0.01 \sigma^2$.

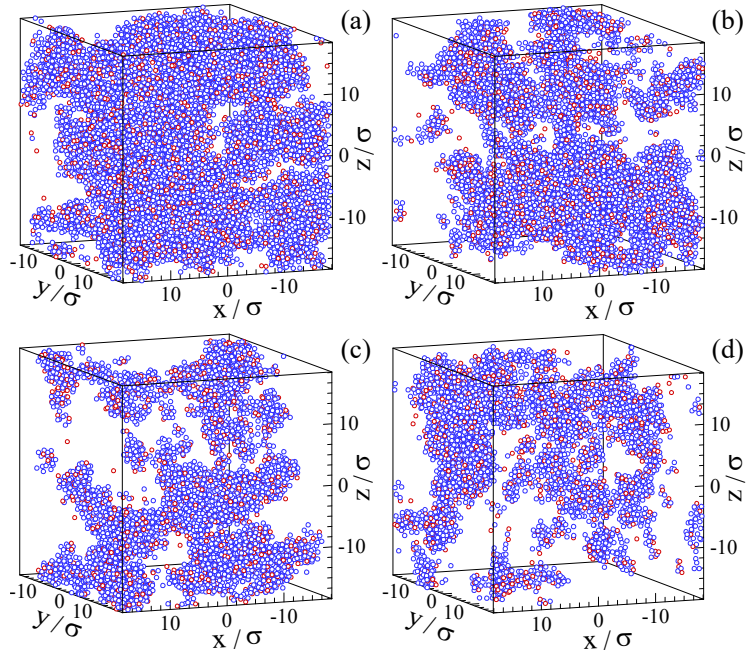


FIG. 10: (Color online) Instantaneous positions of atoms of types A and B for the strain amplitude $\gamma_0 = 0.07$, temperature $T_{LJ} = 10^{-5} \varepsilon/k_B$, and nonaffine measure (a) $D^2(19T, T) > 0.01 \sigma^2$, (b) $D^2(79T, T) > 0.01 \sigma^2$, (c) $D^2(199T, T) > 0.01 \sigma^2$, and (d) $D^2(599T, T) > 0.01 \sigma^2$.